Su Hui (Orcid ID: 0000-0003-1265-9702)

Wu Longtao (Orcid ID: 0000-0001-8447-8180)

Jiang Jonathan, H (Orcid ID: 0000-0002-5929-8951)

Neelin J. David (Orcid ID: 0000-0001-9414-9962)

Observed Tightening of Tropical Ascent in Recent Decades and Linkage to Regional Precipitation Changes

Hui Su[1], Longtao Wu[1], Chengxing Zhai[1], Jonathan H. Jiang[1], J. David Neelin[2], Yuk L. Yung[3]

[1]Jet Propulsion Laboratory, California Institute of Technology, Pasadena, CA 91109, USA

[2]Department of Atmospheric and Oceanic Sciences, University of California, Los Angeles, Los Angeles, CA 90095, USA

[3]Division of Geological and Planetary Sciences, California Institute of Technology, Pasadena, CA 91125, USA

Corresponding author email: Hui.Su@jpl.nasa.gov

This article has been accepted for publication and undergone full peer review but has not been through the copyediting, typesetting, pagination and proofreading process which may lead to differences between this version and the Version of Record. Please cite this article as doi: 10.1029/2019GL085809

Key Points:

1. Tropical ascent area has been decreasing at a rate about –1% decade^{-1} from 1979 to 2016
2. Associated with tropical ascent tightening, rain rate in the top 1% of monthly rainfall in the tropics has been increasing at 1.1% decade^{-1}
3. Southeast Amazon experiences a drying trend of about –3.2% decade^{-1} related to tropical ascent tightening from 1979 to 2016

Abstract. Climate models predict that the tropical ascending region should tighten under global warming, but observational quantification of the tightening rate is limited. Here we show that the observed spatial extent of the relatively moist, rainy and cloudy regions in the tropics associated with large-scale ascent has been decreasing at a rate of −1% decade^{-1} (−5% K^{-1}) from 1979 to 2016, resulting from combined effects of interdecadal variability and anthropogenic forcings, with the former contributing more than the latter. The tightening of tropical ascent is associated with an increase in the occurrence frequency of extremely strong ascent, leading to an increase in the average precipitation rate in the top 1% of monthly rainfall in the tropics. At the margins of the convective zones such as the Southeast Amazonia region, the contraction of large-scale ascent is related to a long-term drying trend about −3.2% decade^{-1} in the past 38 years.

Plain Language Summary: The ascending branch of the tropical circulation is tied to the inter-tropical convergence zone (ITCZ) and encompasses the climatologically wettest area with heavy rainfall and abundant convective clouds. Climate models suggest that the tropical ascent area should tighten under global warming; however, observational evidence of the tightening is limited. We analyze three leading reanalysis datasets and three direct observables as proxies of large-scale ascent in recent decades. We find that the area coverage of the tropical ascending region has been decreasing at a rate of −1% decade^{-1} from 1979 to 2016. The observed tightening is largely driven by natural climate variability and anthropogenically forced global warming plays a secondary role. The tightening of tropical ascent is associated with an increase in the average precipitation rate in the top 1% of monthly rainfall in the tropics. At the margins of the convective zones such as the Southeast

Amazonia region, the contraction of large-scale ascent is related to a drying trend about -3.2% decade^{-1} in the past 38 years. The regional expression of the tropical ascent tightening has profound hydrological impacts in such locations.

1. Introduction

Large-scale circulation in the tropics including the Hadley Cell and Walker Cell plays an important role in transporting energy, moisture, and momentum in Earth's climate system. Changes to the large-scale circulation under global warming are closely linked to global and regional energy and water cycles. Climate models predict that the ascending branch of the Hadley Circulation tends to narrow with surface warming (Su et al; 2014; Lau and Kim, 2015; Byrne and Schneider, 2016; Su et al., 2017), while the descending branch expands poleward (Hu and Fu, 2007; Lu et al., 2007; Seidel et al., 2008). The tightening of the tropical ascent is consistent with the thermodynamic scaling argument that convective mass flux would reduce in a warmer climate (Held and Soden, 2006). It can also be explained by the "upped-ante mechanism" that postulates the margins of convective zones would experience suppressed convective initiation because increased convective threshold associated with warmer tropospheric temperature would be less frequently satisfied due to limited moisture supply (Neelin et al., 2003). Byrne and Schneider (2016) showed that the negative moist static energy (MSE) advection by the zonal-mean flow acting on the strengthened MSE meridional gradient between the moist tropics and the dry subtropics contributes primarily to the narrowing tendency of the Inter-Tropical Convergence Zone (ITCZ) in the models that participated in the Coupled Model Intercomparison Project Phase 5 (CMIP5). However, the magnitudes of the narrowing vary substantially across the models, which affect the model simulations of tropical high-altitude cloud cover and thus atmospheric radiative cooling rate and global-mean precipitation sensitivity to surface warming (Su et al., 2017).

Although most climate models agree on the sign of the tropical ascent area change when climate warms, the magnitudes of the tightening differ substantially (Byrne and Schneider, 2016; Su et al., 2017; Su et al., 2019). Observational assessment of the tropical ascent area change is needed to constrain the model simulations. During the satellite era since 1979, global-mean surface temperature (T_s) has increased about 0.2 K decade^{-1}, primarily caused by anthropogenic radiative forcing associated with increasing greenhouse gases (GHG) (IPCC 2013). Internal climate variability such as the Pacific Decadal Oscillation (PDO) and Atlantic Multidecadal Oscillation (AMO) modulates the warming trend over certain periods (Gu et al., 2016). It is not clear whether the spatial extent of the tropical ascending region has experienced discernible changes in accordance with the long-term warming. Wodzicki and Rapp (2016) used precipitation data from the Global Precipitation Climatology Project (GPCP) and Tropical Rainfall Measuring Mission (TRMM) supplemented by reanalysis low-level divergence and potential temperature fields to define the location, width and strength of the ITCZ in the tropical Pacific. They found that the ITCZ experienced narrowing and strengthening from 1979 to 2014 and the narrowing trends vary at different longitudinal locations.

In this study, we examine the long-term trends in tropical ascent area represented in three leading reanalysis datasets and three direct observables as proxies of large-scale ascent in recent decades. The associated spatial patterns of the precipitation changes are analyzed in both observations and CMIP5 model simulations, noting certain regions of particular sensitivity.

2. Data and Methods

The three reanalyses we use are the European Centre for Medium-Range Weather Forecasts (ECMWF) interim analysis (ERA-I, Dee et al., 2011), the Modern-Era Retrospective analysis for Research and Applications, version 2 (MERRA-2, Gelaro et al., 2017), and the Japanese 55-year ReAnalysis (JRA-55, Kobayashi et al., 2015). We define the tropical ascending region by vertical pressure velocity at 500 hPa less than zero ($\omega_{500} < 0$ Pa s^{-1}) (Figure S1a). Note that

this definition of tropical ascent area is different from previous studies that focused on the meridional width of zonal-mean Hadley Circulation (e.g., Byrne and Schneider, 2016) or the commonly-used ITCZ width (Wodzicki and Rapp, 2016). It represents a holistic measure of the tropical ascent area, regardless of the zonally-symmetric or zonally-asymmetric components. Su et al. (2019) elaborates the usefulness of this simplified definition in understanding of the basic mass and energy balance of the tropics.

As ω_{500} is dynamically inferred from other observational constraints in the reanalysis models rather than a direct observation, we identify a few proxies of tropical ascent that are measured directly or are tightly constrained by instrument observerables. These proxies are atmospheric column relative humidity (CRH), evaporation minus precipitation (E−P) and outgoing longwave radiation (OLR) because their connections with large-scale circulation are well established (Bretherton et al., 2004; Chen et al., 2002; Byrne and Schneider 2016).

The CRH is defined as the ratio between column-integrated precipitable water (PW) and saturation PW (PWs) and the latter is calculated by the vertical integral of saturation water vapor at each pressure level as a function of tropospheric temperature and pressure from the surface to 100 hPa. Previous studies showed that precipitation has a strong relation with high CRH over tropical oceans (Bretherton et al., 2004). We use PW and PWs from the three reanalyses because both PW and tropospheric temperature are constrained in reanalysis by assimilating satellite radiances that are sensitive to atmospheric temperature and moisture content. We use CRH ≥ 60% to represent the tropical ascending region (Figure S1b).

Based on atmospheric moisture budget, the regions with precipitation greater than evaporation (E−P < 0) require net moisture convergence and ascending motion. Using the precipitation estimates from the GPCP (Huffman et al., 2009) and evaporation from the Objectively Analyzed air-sea Fluxes (OAFlux) for the Global Oceans project (Yu and Weller, 2007), we find the boundary of the tropical ascending zone extends wider than the contour of

E−P < 0 because of the effect of moisture advection. Instead, E−P ≤ 1 mm day^{-1} yields better correspondence to the ascent over the tropical oceans (Figure S1c).

Furthermore, as the tropical convergence zone is associated with abundant convective clouds and low OLR, we use OLR ≤ 250 W m^{-2} as an additional index of tropical ascent based on the spatial distributions of OLR and ω_{500} (Figure S1d). The NOAA interpolated OLR from 1979 to 2016 (Liebmann and Smith, 1996) is used.

Table S1 lists the sources and resolutions of the observational datasets. The Hadley Centre and Climate Research Unit surface temperature 4.4.0.0 (HadCRUT4) dataset (Morice et al., 2012) is used. Our trend analysis results are qualitatively insensitive to the choices of threshold values for the three proxy datasets.

Besides observational data, we employ 24 climate model simulations available at the CMIP5 archive (Taylor et al., 2012). Three types of model simulations are analyzed: the AMIP-type runs driven by the observed sea surface temperature (SST) and sea ice from 1979 to 2008, the atmosphere-ocean coupled historical runs driven by natural and anthropogenic forcings from 1979 to 2005, and the projected RCP4.5 runs from 2006 to 2100 (see Table S2).

All analyses are conducted over the tropics (30°S-30°N) including both land and ocean except for E−P, for which only ocean data are available. The annual-mean area coverage of the tropical ascent is based on the monthly mean data where the conditions for ascent are satisfied. The respective climatological annual means are removed in the yearly time series of tropical ascent area. All observational datasets are from January 1979 to December 2016, except that the MERRA-2 reanalysis starts from January 1980. The linear trends in all variables are computed using the least squares linear regression that minimizes chi-square error.

3. Results

3.1 Robust tightening of tropical ascent area in recent decades

Figure 1 shows the area fractions of the tropical ascending region based on the aforementioned indicators all demonstrate a decreasing trend. The tropical ascending area fractions represented by $\omega_{500} < 0$ Pa s^{-1} in the three reanalyses exhibit a trend around −0.1% $decade^{-1}$ with large uncertainties (Figure 1a). The ascent area fractions indicated by ERA-I CRH ≥ 60%, observed E−P ≤ 1 mm day^{-1} or OLR ≤ 250 W m^{-2} display larger negative trends (Figure 1b) ranging from −0.3% to −0.4% $decade^{-1}$. The units of % $decade^{-1}$ refer to the percentage of the ascent area out of the entire tropics from 30°S to 30°N. Using MERRA-2 or JRA-55 CRH (Figures S2 and S3), the narrowing trend of the tropical moist area is considerably higher, −1.2% $decade^{-1}$ or −0.6% $decade^{-1}$ respectively, due to the differences in the assimilation modeling systems and observational datasets used. Despite the differences between the datasets, a robust decreasing trend is found in the spatial extent of the tropical ascending region for all indices. Out of the three proxy data, the ascent area fraction based on E−P ≤ 1 mm day^{-1} yields the strongest negative trend with the lowest uncertainty, −0.38% ± 0.15% $decade^{-1}$. Given the large unceratinties in the reanalysis vertical velocity field, the long-term trends from CRH, E−P and OLR are likely more reliable. The averaged tightening trend from the three proxy datasets is approximately −0.3% ± 0.2% $decade^{-1}$ (Figure 1b), which is about −1% $decade^{-1}$ relative to climatology or −5% K^{-1} when normalized by global-mean T_s trend.

The long-term trends in the tropical ascent area based on $\omega_{500} < 0$ Pa s^{-1} or E−P ≤ 1 mm day^{-1} from all the model simulations are shown in Table S2. The simulated trends based on CRH or OLR indicators are analyzed, but they exhibit larger inter-model differences and thus are not shown. Using E−P ≤ 1 mm day^{-1} to define the ascent area, we find that the multi-model-mean of the AMIP runs from 1979 to 2008 is within one-standard deviation of the observed tightening trend of −0.38% ± 0.15% $decade^{-1}$ from 1979 to 2016 (Figure 2). The multi-model-means of the coupled historical runs and RCP4.5 runs produce a tightening trend only 20% of

the AMIP ensemble mean (Figure 2), although the three types of model simulations possess similar global-mean T_s trends with 0.16 K, 0.23 K, and 0.19 K decade^{-1} for the AMIP, historical, and RCP4.5 multi-model-means, respectively. The differences in the tightening trends are associated with a pattern of SST changes in the observation that differ substantially from the ensemble-average trends in the historical and RCP4.5 coupled runs (Figure 2 insets). The observed surface cooling in the eastern Pacific due to the negative phase of the PDO in the second half of the record, affects the SST gradient and thus tropical circulation intensity. Enhanced SST gradient in the AMIP runs leads to a strengthened tropical circulation and a greater tightening of ascent area (Su et al., 2019). The multi-model-mean of the coupled historical runs minimizes the effects of the SST anomalies associated with the decadal-to-multidecadal climate variability while approximately capturing the forced long-term warming (Figure 2 insets). Given that the AMIP simulations with observed SST approximately capture the observed tightening magnitude we infer that the observed tropical ascent tightening in recent decades is mainly contributed by natural climate variability. The tightening trends in the coupled simulations suggest there is indeed a tightening tendency associated with external forcing primarily driven by increasing GHG, but this is smaller, about 20% of the trend in the AMIP ensemble average. Over a longer time scale, e.g., about 100 years, the effect of decadal-to-multidecadal climate variability becomes less important and the role of the GHG-forced surface warming would dominate, as in the RCP4.5 runs (Figure 2). The qualitative consistency in terms of the sign of the trends in the 24 AMIP runs (only one model produces a positive trend) corroborates the robustness of the tropical ascent tightening in recent decades. Similar results are found when $\omega_{500} < 0$ Pa s^{-1} is used to define the ascending region in the models (Table S2).

Even with the same SST patterns in all the AMIP runs, the differences in the model physics, especially the moist convective schemes (Schiro et al., 2019), can still create large inter-model

spread in the tightening trend, as shown in Figure 2 and Table S2. Su et al. (2019) found that model differences in the cloud radiative effects at the top of atmosphere (TOA) over deep convective regions are highly correlated with the diverse responses in the ascent intensity and area changes, indicating a strong coupling between circulation and clouds.

3.2 Linkages of tropical ascent tightening to regional precipitation changes

As precipitation variations are strongly influenced by changes in large-scale circulation, it is expected that the tightening of tropical ascent in recent decades would manifest in global and regional water cycle changes. Employing the conditional sampling approach (e.g., Bony et al., 2004; Su et al., 2013) in which the tropical mean precipitation is expressed as an integral of precipitation rate in each circulation (represented by ω_{500}) regime, p(ω), weighted by the probability density function (PDF) of ω_{500}, f(ω), as shown in Eq (1), the impacts of the tropical ascent tightening on precipitation change can be readily disclosed.

Denoting the tropical mean precipitation rate as P, we have

$$P = \int_{-\infty}^{\infty} p(\omega) f(\omega) d\omega. \qquad (1)$$

Following Emori and Brown (2005), the change of precipitation with time (t) or T_s can be decomposed into a thermodynamic component (the first term on the r.h.s. of Eq. 2), a dynamic component (the second term on the r.h.s. of Eq. 2) and the co-variant (the third term on the r.h.s. of Eq. 2), whereas overbar denotes the climatological mean values,

$$\frac{dP}{dt} = \int_{-\infty}^{\infty} \frac{dp(\omega)}{dt} \overline{f(\omega)} d\omega + \int_{-\infty}^{\infty} \overline{p(\omega)} \frac{df(\omega)}{dt} d\omega + \int_{-\infty}^{\infty} \frac{dp(\omega)}{dt} \frac{df(\omega)}{dt} d\omega. \qquad (2)$$

The thermodynamic component is associated with the increase of water vapor when T_s increases assuming that the circulation is unchanged; the dynamic component is related to the change of circulation assuming that the moisture content is unchanged. The co-variant term is generally smaller than the first two terms.

Dividing the full circulation regime into 20 equal occurrence bins with each bin accounting for 5% occurrence, we examine the long-term trends of f(ω) in three reanalysis datasets in recent decades (Figure 3). The cut-off values of ω_{500} for each bin differ slightly for different reanalysis datasets. Only the ones for ERA-I are labeled in Figure 3. Climatological precipitation rate p(ω) in each ω_{500} bin is displayed in grey bars based on GPCP precipitation and ERA-I ω_{500} (Figure 3).

The distribution of p(ω) shows that precipitation decreases monotonically from strongly ascending to descending regimes and heavy precipitation is associated with strong ascent. Over the past 38 years, the three reanalysis datasets yield different trends in each ω_{500} bin; however, a common feature shared by all three datasets is that the occurrence of extremely strong ascent (the highest 5% of negative ω_{500}) has increased, while the occurrence of moderate ascent has decreased, corresponding to a strengthening and tightening of tropical ascent. Therefore, the dynamic component of precipitation change would cause a shift from moderate to extremely heavy rain rate (Eq. 2). Combined with the thermodynamic increase of precipitation at a rate of about 7% K^{-1} governed by the Clausius-Clapeyron relation, we expect that the occurrence of extremely heavy precipitation in the tropics would increase markedly.

Indeed, the GPCP precipitation data confirm this expectation. Figure 4a shows the mean precipitation rate in the highest 5% ascent bin increases at a rate of 0.37 mm day^{-1} $decade^{-1}$ (about 4% $decade^{-1}$ or 20% K^{-1} relative to the long-term mean of 9.4 mm day^{-1}), while the mean precipitation rate in the top 1% of monthly precipitation over the tropics increases in tantem at a rate of 0.2 mm day^{-1} $decade^{-1}$ (about 1.1% $decade^{-1}$ or 5.5% K^{-1} relative to the long-term mean of 17 mm day^{-1}) from 1979 to 2016. The correlation coefficient (R) between the two measures of tropical heavy precipitation is 0.72, statistically significant at 99% level. It suggests that the dynamically driven precipitation change due to the increase of extremely strong ascent contributes substantially to the intensifying extremely heavy rainfall. Compared to the

climatological global-mean precipitation rate of 2.2 mm day^{-1}, the heavy monthly rain rates of 8.5 mm day^{-1} and higher shown in Figure 4a are likely associated with frequent or extreme floods. Over land, a steady increase of extreme precipitation on the decadal time scale would be catastrophic to regional infrastructure, water resource management, economy and human life.

Figure 4b shows CMIP5 AMIP and historical simulations of the trends in the averaged precipitation rate in the top 1% of monthly means in the tropics scattered against the modeled long-term trends of tropical ascent area. A strong negative correlation exists for all the simulations (R = –0.61 for AMIP and –0.74 for historical runs, statistically significant at 99% level). The observed trends are also close to the linear approximation. This suggests that the models with stronger tightening trends tend to have greater increases of extremely heavy precipitation, as a stronger tightening corresponds to a greater increase in ascent strength due to the mass balance (Su et al., 2019). The model results further demonstrates the relevance of tropical ascent area change to extreme precipitation.

On the other hand, at the edges of the tropical ascending zones, the contraction of tropical ascent would lead to a decrease in ascent occurrence in these regions, a negative $f(\omega<0)$, which would cause a reduction in precipitation due to the dynamic component per Eq (2). In the past decades, a contraction of convective boundary occurs at the eastern edge of equatorial SPCZ, the northern edge of Central America, and the southeastern edge of the Amazonian convergence zone (Figure S4), approximately captured by CMIP5 models (Figures S5 and S6). We specifically examine the Southeast Amazonia region (60°W-30°W, 0°-20°S) as precipitation is vital to biodiversity and agriculture there, and the region has been found sensitive to the low-level inflow of dry air (Lintner and Neelin, 2010) and is thus susceptible to suppression of convection due to the upped-ante mechanism (Neelin and Su, 2005). All four seasons were analyzed and the ascent area tightening over the Amazon was found more

conspicuous during the wet seasons in September, October and November (SON) and December-January-February (DJF) than during the dry seasons (Figures S4 and S7). Furthermore, the CMIP5 simulations for SON are generally more consistent with the observations than other seasons (Figures S5 and S6). Hence, we focus on the results during SON to illustrate the impact of tropical ascent tightening on regional hydrological cycle.

Figure 4c shows the yearly precipitation and ascent area fraction time series over the Amazonia region during SON. There is a clear drying trend about –3.2% decade^{-1} and a decreasing trend in the ascent area fraction. The interannual variations of the regionally-averaged rainfall is highly correlated with the ascent area fraction (R=0.71, Figure 4c). Similar correlations are found for other seasons and in annual mean (Figure S7). To test whether the decrease in precipitation over the Amazonia is related to the tropical-wide ascent area decrease, we examine the CMIP5 simulated Amazonia precipitation trends during SON and find that their magnitudes are highly correlated with the tropical ascent area trends across the models (R=0.55 for AMIP and historical runs together, statistically significant at 99% level) (Figure 4d). The positive correlation between the Amazonia precipitation trends and tropical ascent area trends suggest that the drying in the Amazonia is likely a regional consequence of large-scale tropical circulation change. Previous studies (Neelin et al., 2006; Fu et al., 2013) indicated that the long-term droughts and increased dry-season length in Southern Amazonia may be a response to global warming. Our analysis suggests that the tightening of tropical ascending area associated with increasing GHG would cause a drying trend in the Southeast Amazonia; however, the observed drying in recent decades is likely a combined effect from both GHG forcing and natural climate variability with the latter dominating over the former. Nevertheless, as the tightening of tropical ascent is projected to occur on the centennial time scale, a persistent drying in the Southeast Amazonia would require advance planning to deal with ever-decreasing local water resources.

4. Conclusion and Discussions

The tropical ascending region encompasses the climatologically wettest area with heavy rainfall and abundant convective clouds. Although the tropical ascending region accounts for only ~20% of the global area, the averaged rain rate within this region is about 2.6 times the global-mean, nurturing a rich biodiversity in the land areas.

We find that the moist tropics has become tighter in the past decades. The tightening is associated with a shift from moderate ascent to extremely strong ascent in the circulation regimes, leading to an increase in extremely heavy precipitation in the top 1% in monthly precipitation pdf with rain rate > 16 mm day^{-1}. In the meantime, formerly wet regions at the boundary of the ascending zone such as the Southeast Amazonia region have experienced long-term drying as the tropical ascending area contracts. Our analysis of the CMIP5 model simulations suggests that anthropogenic forcings are partly responsible for the contraction of the ascending area, while the decadal-to-multi-decadal climate variability such as the PDO accounts for about 80% of the observed tightening in recent decades. Moreover, the tightening trend will continue in concert with the increasing GHG despite interannual and decadal oscillations. In parts of the tropics where human life and ecosystems heavily depend on precipitation, the contraction of the ascending regions would have severe impacts on agriculture, forestry, biodiversity and economy. The monotonic surface warming caused by increasing GHG would eventually surpass the internally driven variability and the tightening of moist tropics would persist if no mitigation of the rise of GHG is materialized.

The observed tightening trends based on various indices should serve as a reference to constrain climate models simulations. Given the broad implications of the tropical ascent area changes for global and regional hydrological cycles (Su et al., 2017; Su et al., 2019), we propose that the ascent area metrics based on ω_{500}, CRH, E−P and OLR, as examined in this study, be incorporated into the standard evaluation of climate model performance. The large

discrepancies in model simulations of the tightening trends underscore the pressing need to improve model physics, especially those related to moist convection.

Data Statement. The original reanalysis datasets, observations, and CMIP5 model simulations used in this study are all publicly available. The websites to download these data are:

ERA-I: http://apps.ecmwf.int/datasets/data/interim-full-moda/levtype=sfc/

MERRA-2: https://gmao.gsfc.nasa.gov/reanalysis/MERRA-2/data_access/

JRA-55: https://rda.ucar.edu/datasets/ds628.1/#description

GPCP precipitation: https://www.esrl.noaa.gov/psd/data/gridded/data.gpcp.html

OAFlux: http://oaflux.whoi.edu/data.html

NOAA OLR: https://www.esrl.noaa.gov/psd/data/gridded/data.interp_OLR.html

HadCRU4 T_s: http://www.metoffice.gov.uk/hadobs/hadcrut4

CMIP5: http://cmip-pcmdi.llnl.gov/cmip5/

The methods to process the data and generate the results are described in detail in the paper. Please contact the corresponding author at Hui.Su@jpl.nasa.gov for any questions.

Acknowledgments. This work was performed at Jet Propulsion Laboratory, California Institute of Technology, under contract with NASA. This study is supported by NASA ACMAP-AST and MAP projects. JDN is supported by the NSF AGS-1540518 grant.

References

1. Bony, S., Dufresne, JL., Le Treut, H. et al. Climate Dynamics (2004) 22: 71. https://doi.org/10.1007/s00382-003-0369-6.
2. Bretherton, C. S., M. E. Peters, and L. E. Back, Relationships between water vapor path and precipitation over the tropical oceans. J. Climate, 17, 1517-1528, (2004).
3. Byrne, M. P., and T. Schneider, Narrowing of the ITCZ in a warming climate: Physical mechanisms, Geophys. Res. Lett., 43, 11,350–11,357, doi:10.1002/2016GL070396 (2016).
4. Chen, J., B.E. Carlson, and A.D. Del Genio, Evidence for strengthening of the tropical general circulation in the 1990s. *Science*, 295, 838-841, doi:10.1126/science.1065835 (2002).
5. Dee, D. P., Uppala, S. M., Simmons, A. J., Berrisford, P., Poli, P., Kobayashi, S., Andrae, U., Balmaseda, M. A., Balsamo, G., Bauer, P., Bechtold, P., Beljaars, A. C. M., van de Berg, L., Bidlot, J., Bormann, N., Delsol, C., Dragani, R., Fuentes, M., Geer, A. J., Haimberger, L., Healy, S. B., Hersbach, H., Hólm, E. V., Isaksen, L., Kållberg, P., Köhler, M., Matricardi, M., McNally, A. P., Monge-Sanz, B. M., Morcrette, J.-J., Park, B.-K., Peubey, C., de Rosnay, P., Tavolato, C., Thépaut, J.-N. and Vitart, F., The ERA-Interim reanalysis: configuration and performance of the data assimilation system. Q.J.R. Meteorol. Soc., 137: 553–597. doi:10.1002/qj.828, (2011).
6. Emori, S., and S. J. Brown, Dynamic and thermodynamic changes in mean and extreme precipitation under changed climate. *Geophys. Res. Lett.*, **32**, L17706, doi:https://doi.org/10.1029/2005GL023272 (2005).
7. Fu, R. L. Yin, W. Li, P. Arias, R. E. Dickinson, L. Huang, S. Chakraborty, K. Fernandes, B. Liebmann, R. Fisher, and R. B. Myneni, Increased dry-season length over southern

Amazonia in recent decades and its implication for future climate projection. Proc. Natl Acad. Sci. USA 110, 18110–18115 (2013).

8. Gelaro, R., and Coauthors, The Modern-Era Retrospective Analysis for Research and Applications, version-2 (MERRA-2). J. Climate, 30, 5419–5454, doi:https://doi.org/10.1175/JCLI-D-16-0758.1. (2017).
9. Gu, G., Adler, R.F. & Huffman, Long-term changes/trends in surface temperature and precipitation during the satellite era (1979–2012), Clim Dyn, 46: 1091. https://doi.org/10.1007/s00382-015-2634-x, (2016).
10. Gu, G., R. F. Adler, Interdecadal variability/long-term changes in global precipitation patterns during the past three decades: global warming and/or Pacific decadal variability? Clim Dyn 40:3009–3022. doi:10.1007/s00382-012-1443-8 (2013).
11. Held, I. M., and B. J. Soden, Robust responses of the hydrological cycle to global warming, *J. Clim*., 19, 5686–5699 (2006).
12. Hu, Y. & Fu, Q. Observed poleward expansion of the Hadley circulation since 1979. Atmos. Chem. Phys. 7, 5229–5236 (2007).
13. Huffman, G.J, R.F. Adler, D.T. Bolvin, G. Gu, Improving the Global Precipitation Record: GPCP Version 2.1. *Geophys. Res. Lett*., 36,L17808, doi:10.1029/2009GL040000 (2009).
14. IPCC, 2013: Climate Change 2013: The Physical Science Basis. Contribution of Working Group I to the Fifth Assessment Report of the Intergovernmental Panel on Climate Change. Cambridge University Press, Cambridge, UK and New York, NY, 1535 pp. http://www.climatechange2013.org/report/
15. Kobayashi, S., Y. Ota, Y. Harada, A. Ebita, M. Moriya, H. Onoda, K. Onogi, H. Kamahori, C. Kobayahsi, H. Endo, K. Miyaoka, K. Takahashi, The JRA-55 Reanalysis: General Specifications and Basic Characteristics, Journal of the Meteorological Society

of Japan. Ser. II, Online ISSN 2186-9057, Print ISSN 0026-1165, https://doi.org/10.2151/jmsj.2015-001 (2015).

16. Lau W. K.-M. & K.-M. Kim, Robust Hadley Circulation changes and increasing global dryness due to CO_2 warming from CMIP5 model projections, *Proc. Nat. Acad. Sci.*, 112 (12), 3630–3635, doi: 10.1073/pnas.1418682112 (2015).
17. Liebmann B. and C.A. Smith, Description of a Complete (Interpolated) Outgoing Longwave Radiation Dataset. Bulletin of the American Meteorological Society, 77, 1275-1277 (1996).
18. Lintner, B. R. and J. D. Neelin: Tropical South America/Atlantic sector convective margins and their relationship to low-level inflow. *J. Clim.*, **23**, 2671-2685, doi:10.1175/2009JCLI3301.1.
19. Lu, J., G. A. Vecchi, and T. Reichler, Expansion of the Hadley cell under global warming, Geophys. Res. Lett., 34, L06805, doi:10.1029/2006GL028443 (2007).
20. Morice, C. P., J. J. Kennedy, N. A. Rayner, and P. D. Jones, Quantifying uncertainties in global and regional temperature change using an ensemble of observational estimates: The HadCRUT4 dataset, J. Geophys. Res., 117, D08101, doi:10.1029/2011JD017187 (2012).
21. Neelin, J. D., C. Chou, and H. Su, Tropical drought regions in global warming and El Nino teleconnections. *Geophys. Res. Lett*.,, 30(24) 2275, doi:10.1029/2003GLO018625 (2003).
22. Neelin, J. D., and H. Su: Moist teleconnection mechanisms for the tropical South American and Atlantic sector during El Niño, J. Climate, 18, 3928-3950 (2005).
23. Neelin, J. D., M. Munnich, H. Su, J. E. Meyerson, and C. E. Holloway, Tropical drying trends in global warming models and observations. Proc. Nat. Acd. Sci., 103, 6110-6115, doi:10.1073/pnas.0601798103 (2006).

24. Schiro, K. A., H. Su, Y. Wang, B. Langenbrunner, J. H. Jiang, and J. D. Neelin, Relationships between tropical ascent and high cloud fraction changes with warming revealed by perturbation physics experiments in CESM, Geophys. Res. Lett., doi:10.1029/2019GL083026 (2019).
25. Seidel, D. J., Q. Fu, W. J. Randel, and T. J. Reichler, Widening of the tropical belt in a changing climate. *Nat. Geosci*., 1, 21–24 (2008).
26. Su, H., et al., Diagnosis of Regime-dependent Cloud Simulation Errors in CMIP5 Models Using "A-Train" Satellite Observations and Reanalysis Data, J. Geophys. Res, 118, 7, 2762-2780, 10.1029/2012JD018575, (2013).
27. Su, H., J.H. Jiang, C. Zhai, T.J. Shen, J.D. Neelin, G.L. Stephens, and L.Y. Yung, Weakening and Strengthening Structures in the Hadley Circulation Change under Global Warming and Implications for Cloud Response and Climate Sensitivity, Journal of Geophysical Research: Atmospheres 119, 10, 5787–5805, doi:10.1002/2014JD021642, (2014).
28. Su, H., J. H. Jiang, J. David Neelin, T. Janice Shen, C. Zhai, Qing Yue, Zhien Wang, Lei Huang, Yong-Sang Choi, Graeme L. Stephens, Yuk L. Yung, Tightening of tropical ascent and high clouds key to precipitation change in a warmer climate, Nature Communications, 8, 15771, doi: 10.1038/ncomms15771 (2017).
29. Su, H., C. Zhai, J. H. Jiang, L. Wu, J. D. Neelin, Y.-L. Yung, A dichotomy between model responses of tropical ascent and descent to surface warming, npj Climate and Atmospheric Science, doi:10.1038/s41612-019-0066-8 (2019).
30. Taylor, K. E., Ronald J. Stouffer, Gerald A. Meehl, An Overview of CMIP5 and the Experiment Design. *Bulletin of the American Meteorological Society*, **93**, 485–498, doi: 10.1175/BAMS-D-11-00094.1. (2012).

31. Wodzicki, K. R., and A. D. Rapp, Long-term characterization of the Pacific ITCZ using TRMM, GPCP, and ERA-Interim, *J. Geophys. Res. Atmos*., 121, 3153–3170, doi:10.1002/2015JD024458 (2016).

32. Yu, L., and R. A. Weller, Objectively Analyzed air-sea heat Fluxes for the global ice-free oceans (1981–2005), *Bull. Am. Meteorol. Soc*., 88, 527–539 (2007).

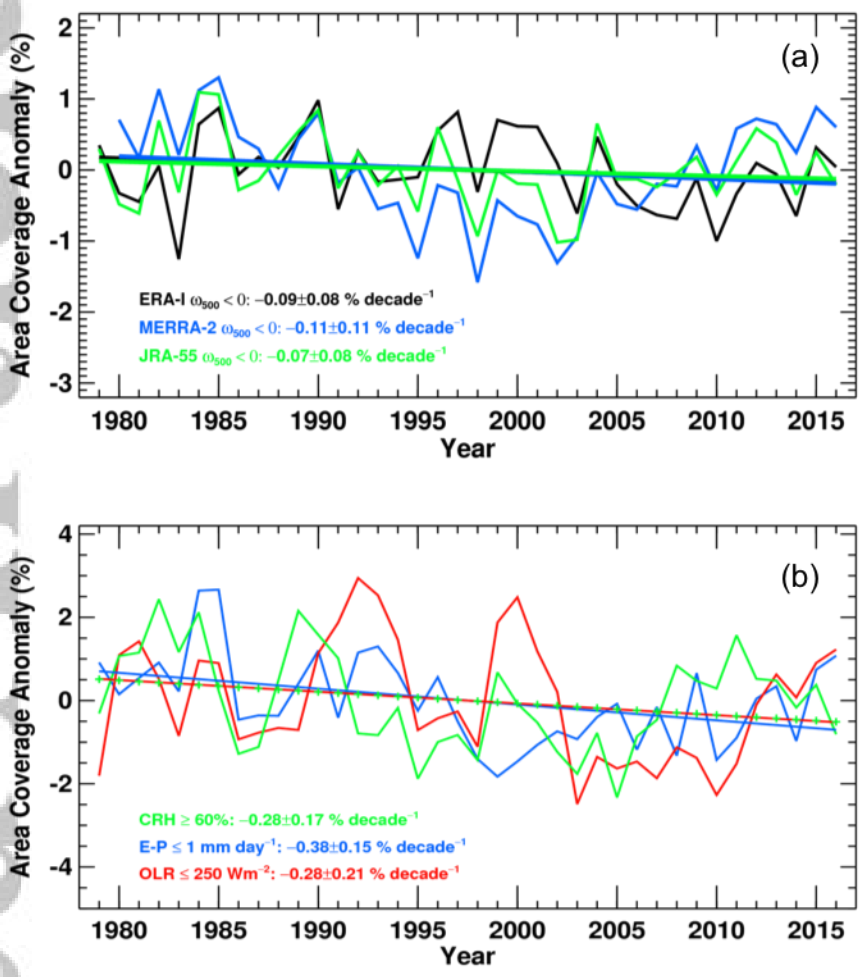

Figure 1. Time evolution of the annual-mean spatial extent of tropical ascending region from 1979 to 2016 represented by (a) $\omega_{500} < 0$ Pa s^{-1} and (b) based on CRH ≥ 60% (in green), E−P ≤ 1 mm day^{-1} (in blue) and OLR ≤ 250 W m^{-2} (in red). The percentage is out of the entire tropics between 30°S-30°N. The respective climatological annual-means are removed from the time series. Linear regression fittings are shown; associated linear trends with one standard deviation are given in the legend.

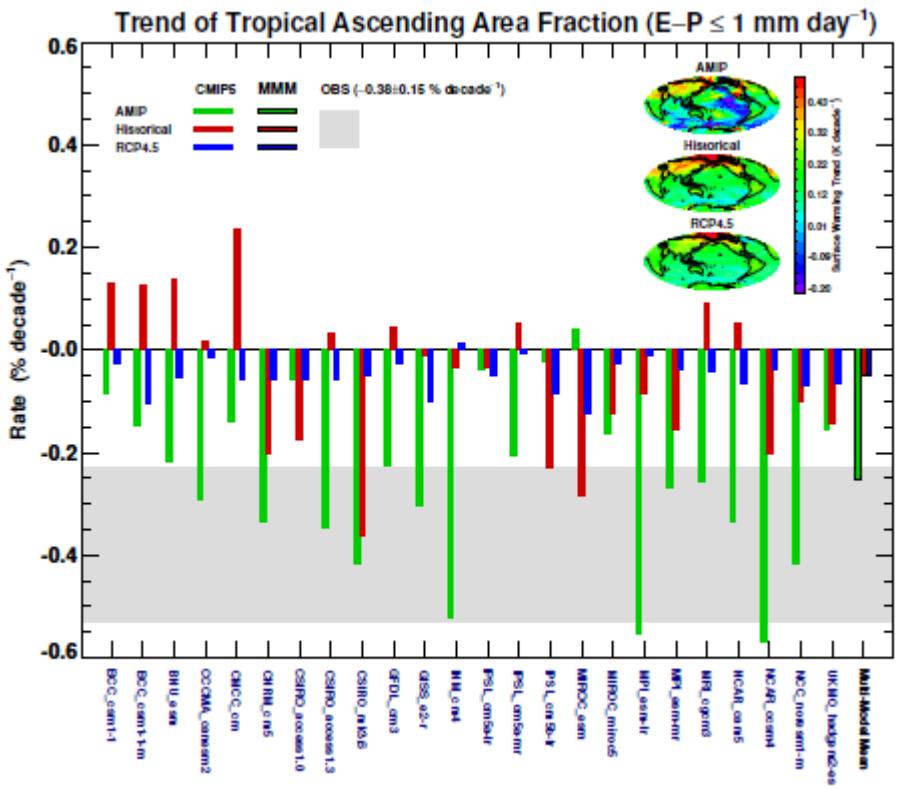

Figure 2. CMIP5 model simulated linear trends of the spatial extent of tropical ascending region based on E−P ≤ 1 mm day^{-1} with AMIP from 1979 to 2008 in green, historical from 1979 to 2005 in red, and the projected RCP4.5 trend from 2006 to 2100 in blue. The multi-model-means are listed in the last column. The observed trend with one standard deviation based on observed E−P ≤ 1 mm day^{-1} is marked in the gray shaded area. The insets show the multi-model-mean spatial distributions of surface temperature trends in the AMIP, historical and RCP4.5 runs.

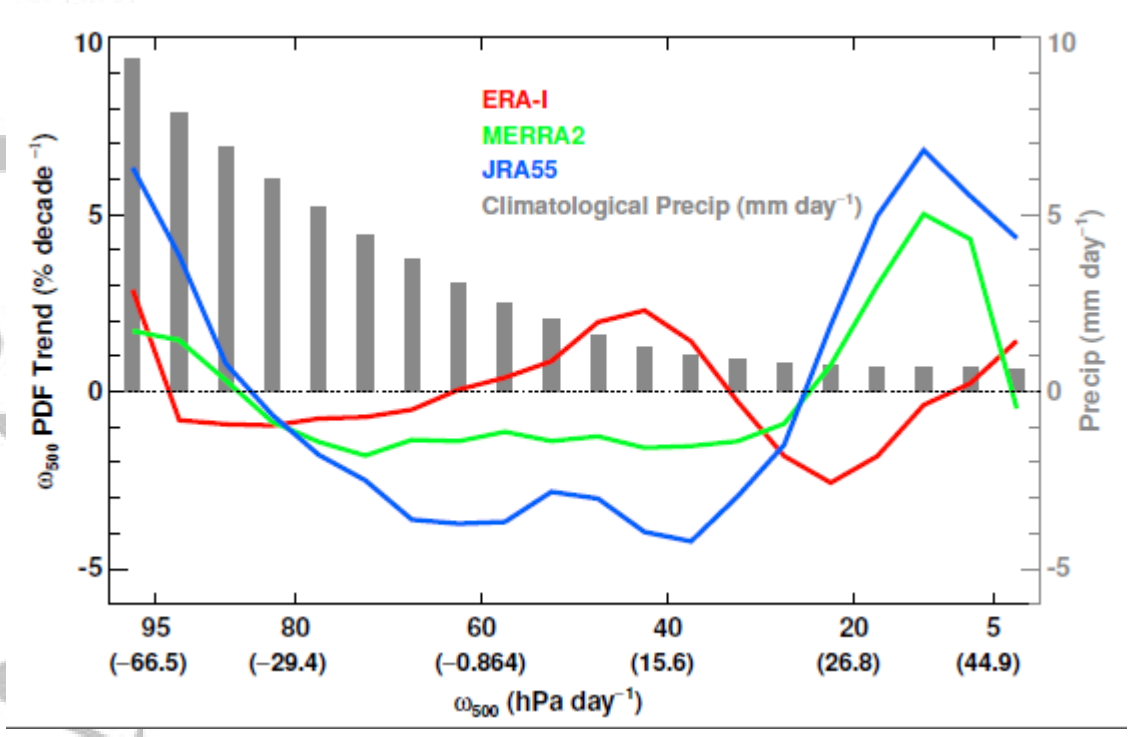

Figure 3. Trends in the occurrence frequency of vertical velocity at 500 hPa (ω_{500}) in 20 ω_{500} bins with 5% occurrence interval for three reanalysis datasets (ERA-I in red, MERRA-2 in green and JRA-55 in blue). The grey bars are climatological rain rates in mm day^{-1} (axis on the right) in each ω_{500} bin using the GPCP precipitation and ERA-I ω_{500}.

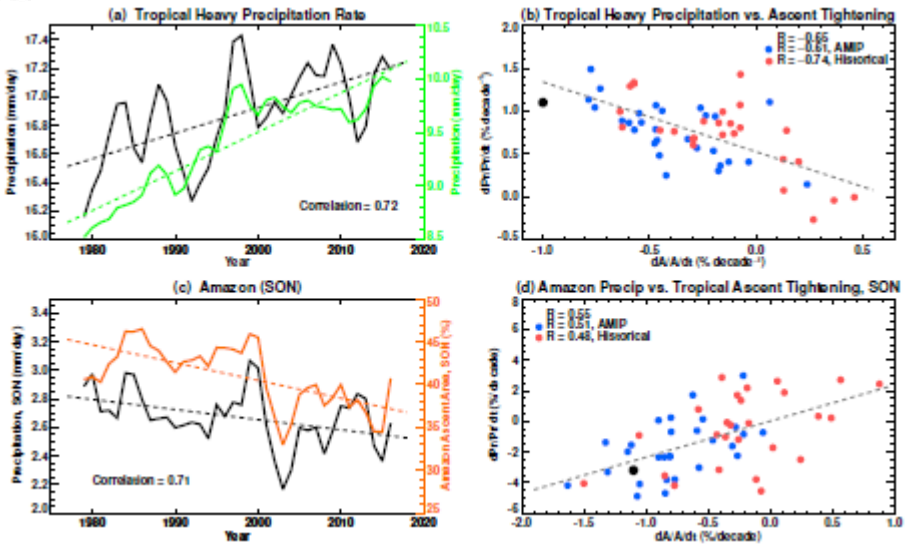

Figure 4. (a) Time series of observed mean precipitation rate in the top 1% of monthly precipitation (black) and mean precipitation rate in the highest 5% ascent bin of ERA-I reanalysis (green). (b) CMIP5 long-term trends in the mean precipitation rate in the top 1% of monthly precipitation scattered against the trends in modeled tropical ascent tightening trends along with the observations in black. (c) Time series of mean precipitation rate over the Southeast Amazonia region from GPCP (black) and the percentage of the ascent area for this region based on ERA-I $\omega_{500} < 0$ (orange) during Sep-Oct-Nov (SON). (d) CMIP5 long-term trends in mean precipitation rate over the Southeast Amazonia region scattered against the trends in modeled tropical ascent tightening trends during SON along with the observations in black. A 3-year running averaging is applied to all the yearly time series. The dashed lines are the least squares linear fits to the data.